Preparation of carbon nanoparticles by plasma assisted pulsed laser deposition method

-size and binding energy dependence on ambient gas pressure and plasma condition-

Y. Suda [a], T. Ono [a], M. Akazawa [a], Y. Sakai [a], J. Tsujino [b], N. Homma [b]

[a] *Graduate school of Engineering, Hokkaido University, Sapporo 060-8628, Japan*

[b] *Hokkaido Electric Power Co., Inc., 2-1 Tsuishikari, Ebetsu 067-0033, Japan*

Abstract

Nanometer-size carbon particles were prepared on a Si substrate using pulsed laser deposition (PLD) assisted by radio frequency (RF) Ar plasma and were compared with ones prepared by PLD in vacuum and Ar gas. In both the plasma and gas ambiences, experiments were carried out in Ar pressure p_{Ar} ranging from 0.13 to 13 Pa. The particle size increased as p_{Ar} increased. However, the size obtained in the RF Ar plasma was approximately 1.5 times larger than that prepared in the Ar gas. An X-ray photoelectron spectroscopy (XPS) analysis revealed that the carbon film

covered by the particles was in an amorphous state. The sp^3/sp^2 carbon ratio of the film was evaluated by deconvolution of XPS carbon (1*s*) spectra into three components, which are attributed to diamond (sp^3), graphite (sp^2) and carbon oxide components. The highest sp^3/sp^2 ratio was 0.4 in the Ar gas and Ar plasma at p_{Ar} = 0.13 Pa. The sp^3/sp^2 ratio decreases monotonously, as the particle size increases. The ratio obtained in the Ar plasma is larger than that in the Ar gas. The effects of p_{Ar} and plasma for nanoparticle characteristic are discussed.

Keywords: Nanoparticle; laser ablation; carbon; RF plasma; amorphous materials

1. Introduction

Pulsed laser deposition (PLD) techniques in rare gas ambiences have been used for nanometer-size particle (nanoparticle) preparation, multi-component thin film deposition and carbon nanotube syntheses [1-3]. As a result of frequent collisions of ablated particles with gas atoms in plume, the particles cool down and form nanoparticles [4]. These nanoparticles are of interest for various fields of device applications, for example, silicon and gallium nitride nanoparticles for luminescent devices [4-6]. Nanoparticle size was controlled by varying ambient gas pressure. Visible photo luminescence (PL) was

observed from them. The wavelength of the PL was shortened as their size decreased [4, 5].

An amorphous carbon (a-C) thin film has been reported to be a promising material in various fields of industrial applications, such as field electron emitters, surface coatings and tribological materials [7-14]. In particular, efficient electron emission was observed from a-C thin films composed of nanoparticles [8]. These film surfaces are also interesting to electrochemical materials and catalyses because of their large surface to volume ratio. Therefore, carbon nanoparticle preparation under the control of their size and physical properties has to be studied further.

In our previous work, we proposed a plasma assisted PLD method and prepared carbon nanoparticles with a diameter of ~ 100 nm in a 53-Pa Ar gas [1]. The nanoparticles were found to be prepared by coagulation with finer particles. This result showed that the plasma assisted PLD was one of the possible production techniques of nanoparticles with the required size and properties.

In the present study, we examine the effect of RF Ar plasma with pressures p_{Ar} varying from 0.13 to 13 Pa, on the growth kinetics of carbon nanoparticles in a laser ablation plume. The size and bonding states of the nanoparticles on a carbon thin film are analyzed using atomic force microscopy (AFM) and X-ray photoelectron spectroscopy (XPS). They are compared with the properties of nanoparticles prepared in vacuum and Ar gas.

2. Experimental

2.1. *Experimental setup and procedure*

The experimental setup of a plasma assisted PLD system is the same as that described in a previous paper [1]. Here, the essential points in the experimental procedure are described briefly. An ArF excimer laser (LAMBDA PHYSIK COMPex 205; wavelength = 193 nm; pulse duration = 20 ns) is used as a light source. The laser beam path is evacuated in order to avoid laser energy loss due to absorption by oxygen molecules in the air. The laser fluence on a target surface is estimated to be 2.1 J/cm^2 (the spot size on the target = 1 mm × 5 mm), considering the reflection coefficient of mirrors and the transmission factor of the window in the light path. The PLD chamber contains a substrate-holder and six target-holders and is evacuated up to 2.7 × 10^{-6} Pa. An RF (f = 13.56 MHz) plasma is generated in a gold-coated coil with a diameter of 113 mm and a height of 25 mm surrounding the target holders. Sintered graphite is taken as the target, and n-type Si (100) as the substrate. The target and substrate spin with approximately 25 and 10 rev./min, respectively. The repetition rate of laser irradiation is 10 Hz. In order to remove contamination from the target surface, the surface is ablated for ~ 10 min before deposition, masking the substrate by a shutter. The native oxide layer on the Si substrate surface is eliminated by immersing the substrate in a solution of hydrofluoric acid. The deposition is continued for 60 min at 100 °C in both the Ar gas and RF plasma. The Ar gas pressure p_{Ar} is varied from 0.13 to 13 Pa, and the RF input power is fixed at 100 W. The distance between the substrate and target d_{st} is fixed to be 20 mm for all the experiments carried out

in this work.

2.2. *Characterization of nanoparticles*

The film surface morphology and the size and number density of the nanoparticles are examined with an atomic force microscope (AFM, Digital Instruments Nanoscope III Dimension 3000). The imaging area and height range of the film are 1 × 1 μm and 0-30 nm, respectively. The AFM is calibrated by probing a standard test grating with a groove of 5 μm in breadth and 180 nm in depth.

The chemical composition and bonding state of the film are analyzed by an X-ray photoelectron spectroscope (XPS, Shimadzu ESCA-3400; X-ray radiation: Mg-K_α (1253.6 eV); pass energy = 75 eV). The carbon (1*s*) spectra are calibrated by a binding energy of Au (4*f*) = 83.6 eV. Au is deposited on the film by vacuum evaporation.

3. Experimental results and discussion

3.1. *Surface morphology analyzed by AFM*

Fig. 1 shows an AFM image of the carbon film surface obtained in vacuum. The surface is quite smooth except for a few spots where particles are deposited. This smooth surface may be obtained, since, in PLD with ArF excimer laser, the size of carbon cluster C_n

and C_n^+ ablated from a graphite target is n = 1-3, and molten droplets are hardly generated [1, 9-12].

Fig. 2 shows AFM images of the film surface deposited in Ar gas and Ar plasma at p_{Ar} = 0.13 and 13 Pa. In the 0.13-Pa Ar gas ambience, small particles of ~ 10 nm are seen in parts on the surface (see Fig. 2 (a)). In the plasma ambience, the entire surface is covered with nanoparticles which are larger than those obtained in the Ar gas. Especially, in the 0.13-Pa Ar plasma, the nanoparticles seem to exist without any coalescence. The particle number density n_p was counted from the AFM images. At p_{Ar} = 0.13 Pa, n_p in the Ar gas was ~ 7.0×10^{10} cm^{-2}, and n_p in the Ar plasma was ~ 7.8×10^{10} cm^{-2}. Though appreciable difference in n_p between both ambiences is not seen, the nanoparticle size prepared in the Ar plasma is larger than that in the Ar gas. At p_{Ar} = 13 Pa, n_p (~ 2.2×10^{10} cm^{-2} in the Ar plasma and ~ 3.7×10^{10} cm^{-2} in the Ar gas) is smaller than those at p_{Ar} = 0.13 Pa, due to coalescence of finer nanoparticles.

The particle radius r is obtained from the sectional view of the AFM image in Fig. 3. Fig. 4 shows r as a function of p_{Ar} for the particles obtained in the Ar gas and Ar plasma ambiences. In both ambiences, r increases in proportion with $p_{Ar}^{1/4}$ for $p_{Ar} < 10$ Pa. However, for $p_{Ar} > 10$ Pa, presumably the particles grow rapidly due to coalescence of finer particles, since in a previous work the r in a 53-Pa Ar gas ambience was ~ 70 nm and in a 53-Pa Ar plasma ambience was 150 nm [1]. The r values of the particles prepared in the Ar plasma is ~ 1.5 times larger than that in the Ar gas. This result may indicate that the plasma assists the coagulation of nanoparticles effectively.

3.2. *XPS Analysis*

The carbon (1*s*) XPS spectra of the film surface are shown in Fig. 5a, b. The broken lines indicate the peak binding energy (BE) of graphite (100% sp^2, 284.5 eV) and diamond (100% sp^3, 285.5 eV) listed in Yamamoto et al. [10]. These values of BE were confirmed, as well, using the present XPS instrument for samples of gold, crystalline graphite and poly crystalline diamond (Kobe steel Ltd.). In both of the Ar gas and plasma ambiences, the BE at p_{Ar}=0.13 Pa is the closest to the BE of diamond (sp^3), and shifts gradually toward the BE of graphite (sp^2) with increasing p_{Ar}. In vacuum the BE shifts to the BE of sp^2 comparing to the case at p_{Ar}=0.13 Pa. Except the case of the 0.13-Pa Ar gas and vacuum ambiences, since the entire film surface is covered with nanoparticle, the C (1*s*) spectra may represent the bonding property of the particles. However, in the case of the vacuum the spectra come from the smooth surface, and in the 0.13-Pa Ar show average properties of the particles and the surface.

Taking the BE of sp^3 and sp^2 carbon and a Gaussian curve fitting method as Mérel et al. [15] and Díaz et al. [16] did, we deconvoluted the C (1*s*) spectra into the sp^3 carbon, sp^2 carbon and carbon oxide components. The background in spectra was removed according to Shirley's method [17]. An example of the deconvolution is shown in Fig. 5c. The sp^3 or sp^2 content is obtained by integration of each component against the binding energy.

The sp^3/sp^2 carbon ratio is shown in Fig. 6. The largest ratio is 0.4 at p_{Ar} = 0.13 Pa. In this figure, any differences between the ratios for both ambiences are hardly seen. In order to understand the dependence of the sp^3/sp^2 carbon ratio on p_{Ar}, we will introduce the

following surface chemistry model [18-21] and related data on kinetic energy ε_{C+} of C_n^+ and C_n (n = 1-3) reported so far [9-12, 22].

The sp^3 content in a-C films was reported to depend on the kinetic energy ε_{C+} of C_n^+ impinging to the substrate [18]. The C_n^+ chemistry in the surface could be explained using the following 'sub-plantation model' [19-21]. In this model, the energy range E_d for impinging C_n^+, where the chemical bond of sp^2 at a sub-surface is displaced by sp^3, was 50-80 eV. Therefore, the sp^3 content varies depending on ε_{C+} values as follows: (1) When ε_{C+} is in the E_d range, C_n^+ penetrates a few layers beneath the surface, 'sub-surface', where original sp^2 bond could be displaced by sp^3. (2) For $\varepsilon_{C+} > E_d$, C_n^+ dissipates its excess energy as heat after penetration to the sub-surface and leaves the sp^2 bond, since the sp^2 bond is more thermally stable than the sp^3 bond. (3) When $\varepsilon_{C+} < E_d$, C_n^+ cannot penetrate to the sub-surface. Then, C_n^+ piles up on the film surface with sp^2 bond.

In the case of PLD with ArF excimer laser, the main ablated species from graphite target were carbon clusters like C_n and C_n^+ (C_n/C_n^+, n = 1-3) and their ε_{C+} increased from 45 eV to 95 eV, as the laser fluence increased from 2×10^7 to 3×10^8 W/cm^2 [9-12, 22]. According to this information, the present ablated species are C_n/C_n^+ (n = 1-3) and have ε_{C+} around ~ 70 eV, since the present ArF laser fluence is ~1.05×10^8 W/cm^2. However, actually, ε_{C+} may have wide distribution, e.g. depending on n (the mass of C clusters). In vacuum C_n/C_n^+ may reach the substrate without any energy loss, however, for $p_{Ar} \geq 10$ Pa, C_n/C_n^+ cool down appreciably due to collision with Ar atoms in the plume, as the collision mean free path for C_n/C_n^+ at p_{Ar} = 1 Pa is roughly estimated to be the same order as the target-substrate distance, d_{st} (= 20 mm). In this sense, ablated C_n/C_n^+ could grow up by the

coagulation each other in the plume for $p_{Ar} > 1$ Pa.

Fig. 6 shows that the sp^3/sp^2 carbon ratio is ~0.4 at $p_{Ar} = 0.13$ Pa, though the ratio at other p_{Ar} is 0.1-0.2, and for $p_{Ar} > 6$ Pa shows a decreasing tendency. We daringly try to explain the characteristics in Fig. 6, taking the aforementioned 'sub-plantation model'. In vacuum, ε_{C+} of ablated C_n^+ has the upper edge of E_d (some parts are in the E_d and others are larger than E_d). Namely, as C_n^+ chemical processes (1) and (2) would occur together. In the case of the 0.13-Pa Ar gas and the 0.13-Pa plasma, as a small part of C_n^+ have a collision chance with Ar atoms, almost all of C_n^+ reach the substrate with ε_{C+} in the E_d range and would take surface chemistry represented by process (1). This is the reason why the sp^3/sp^2 carbon ratio becomes high at $p_{Ar} = 0.13$ Pa. As p_{Ar} increases further, C_n/C_n^+ would lose its energy down to the bottom of E_d by collision with Ar atoms in plume and coagulate efficiently. Therefore, as p_{Ar} increases, the sp^3/sp^2 carbon ratio decreases with p_{Ar} [changing the surface chemistry from process (1) to (3)]. As we discussed above, a 'sub-plantation model' could explain the growing processes of carbon nanoparticles in an ablation plume.

In order to examine the correlation between the AFM and XPS characteristics, using the result of Figs. 4 and 6 the sp^3/sp^2 carbon ratio was plotted as a function of the particle radius r as shown in Fig. 7. It is noticed that the sp^3/sp^2 carbon ratio decreases monotonously with an increase of r, and that the ratio obtained in the Ar plasma is larger than that in the Ar gas. As the collision frequency increases between C_n/C_n^+ and Ar atoms with increasing p_{Ar}, kinetic energy ε_{C+} of C_n/C_n^+ decreases. Consequently, coagulation of the nanoparticle with lower kinetic energy ε_{C+} would occur more frequently. Therefore, larger nanoparticles contain higher sp^2 content comparing with smaller ones, as discussed in a

'sub-plantation model'. The kinetic energy $\mathcal{E}_{C+}$ of C_n^+ in the plasma may be larger than that in the Ar gas because of the existence of the electric field.

3.3. *Growth kinetics of nanoparticles in a plume*

The AFM images of the films in Figs. 1 and 2 show that almost no particles are deposited on the substrate in vacuum, however, in the Ar gas and plasma ambience the surface is covered by the nanoparticles. In the Ar gas ambience C_n/C_n^+ may grow up to a nanometer size particle in plume due to impingement of a lot of C_n/C_n^+ (n = 1-3). However, in the Ar plasma ambience the mechanism of enhancement of the particle growth could be examined taking into account the following discussion made in SiH_4 plasma CVD [23-26], since no information on carbon is available.

In RF SiH_4 plasmas, as increasing plasma density, Si nanoparticles grow up in the following stages. First, Si atoms are clusterized and the cluster grows to a few nanometers in the plasma in the first ~ 100 ms. After that, the particles start to coagulate with each other by Coulomb attractive force between negatively and positively charged particles, and rapidly grow to a size of 50-60 nm. Finally, the coagulation process stops, and the particles continue to grow by molecular sticking as in this stage almost all of the particles are charged negatively [26].

In the present plasma assisted PLD, the ablated species, C_n^+ and electrons would be trapped in the plume for a longer time than the case of conventional PLD. During this period, C_n^+ would nucleate and form nanoparticles by coagulation between charged

particles, as the plasma provides enough electrons and ions.

4. Conclusion

Amorphous carbon nanoparticles were deposited on the silicon substrate using a plasma assisted PLD method. The particles prepared in Ar plasma for the Ar gas pressure $p_{Ar} < 13$ Pa were compared with those prepared in Ar gases. The particle size increased with p_{Ar} with the power of 1/4, and that prepared in the Ar plasma was 1.5 times larger than the case in the Ar gas. The carbon (1*s*) XPS spectra indicated that the present nanoparticle formation could be, qualitatively, explained by a 'sub-plantation model'. The sp^3/sp^2 carbon ratio decreased monotonously with an increase of *r*, and that the ratio obtained in the Ar plasma was larger than that in the Ar gas.

Acknowledgments

The authors would like to express their appreciation to Professor Y. Amemiya for supporting the experimental environment, Professor H. Sugawara, Dr M.A. Bratescu, Dr A. Oda, Mr T. Nishimura at Hokkaido Univ. and Dr T. Mitsueda at Hokkaido Electric Power Co., Inc. for their helpful comments and advice. Our research was supported in part by a Grant-in-Aid (11750245) from the Ministry of Education, Science, Sports and Culture, Japan.

References

[1] Y. Suda, T. Nishimura, T. Ono, M. Akazawa, Y. Sakai, N. Homma, Thin Solid Films 374 (2000) 287.

[2] Y. Yamada, N. Suzuki, T. Makino, T. Yoshida, J. Vac. Sci. Technol., A 18 (2000) 83.

[3] S. Iijima, T. Ichihashi, Nature 363 (1993) 603.

[4] T. Makimura, Y. Kunii, K. Murakami, Jpn. J. Appl Phys. 35 (1996) 4780.

[5] T. Yoshida, S. Takeyama, Y. Yamada, K. Mutoh, Appl. Phys. Lett. 68 (1996) 1772.

[6] T.J. Goodwin, V.J. Leppert, S.H. Risbud, Appl. Phys. Lett. 70 (1997) 3122.

[7] R. Silva, G. A. J. Amaratunga, J. Robertson, W. I. Milne (Eds.), Amorphous Carbon—State of the Art, World Scientific, Singapore, 1998.

[8] C. Wang, A. Garcia, D.C. Ingram, M. Lake, M.E. Kordesch, Electron. Lett. 27 (1991) 1459.

[9] J.J. Gaumet, A. Wakikusa, Y. Shimizu, Y. Tamori, J. Chem. Soc. Farady Trans. 89 (1993) 1667.

[10] K. Yamamoto, Y. Koga, S. Fujiwara, F. Kokai, R.B. Heimann, Appl. Phys., A 66 (1998) 115.

[11] P.T. Murray, D.T. Peeler, J. Electronic Mater. 23 (1994) 855.

[12] T. Yoshitake, T. Nishiyama, H. Aoki, K. Suizu, K. Takahashi, K. Nagayama, T. IEE Jpn. 119-A (1999) 1147.

[13] Y. Taki, O. Takai, Thin Solid Films 316 (1998) 45.

[14] R. Kalish, Y. Lifshitz, K. Nugent, S. Prawer, Appl. Phys. Lett. 74 (1999) 2936.

[15] P. Mérel, M. Tabbal, M. Chaker, S. Moisa, J. Margot, Appl. Surf. Sci. 136 (1998) 105.

[16] J. Díaz, G. Paolicelli, S. Ferrer, F. Comin, Phys. Rev. B 54 (1996) 8064.

[17] D.A. Shirley, Phys. Rev. B 5 (1972) 4709.

[18] V.I. Merkulov, D.H. Lowndes, G.E. Jellison, A.A. Puretzky, D.B. Geohegan, Appl. Phys. Lett. 73 (1998) 2591.

[19] Y. Lifshitz, S.R. Kasi, J.W. Rabalais, Phys. Rev. Lett. 62 (1989) 1290.

[20] Y. Lifshitz, S.R. Kasi, J.W. Rabalais, W. Eckstein, Phys. Rev. B 41 (1990) 10468.

[21] J. Robertson, Diamond Relat. Mater. 2 (1993) 984.

[22] D.H. Lowndes, V.I. Merkulov, A.A. Puretzky, D.B. Geohegan, G.E. JellisonJ, C.M. Rouleau, T. Thundat, Mat. Res. Soc. Symp. Proc. 526 (1998) 325.

[23] L. Boufendi, A. Bouchoule, Plasma Sources Sci. Technol. 3 (1994) 262.

[24] Y. Watanabe, M. Shiratani, T. Fukuzawa, H. Kawasaki, Y. Ueda, S. Singh, H. Ohkura, J. Vac. Sci. Technol. A 14 (1996) 995.

[25] C. Couteille, C. Hollenstein, J.-L. Dorier, P. Gay, W. Schwarzenbach, A.A. Howling, E. Bertran, G. Viera, R. Martins, A. Mararico, J. Appl. Phys. 80 (1996) 2069.

[26] U. Kortshagen, U. Bhandarkar, Phys. Rev. E 60 (1999) 887.

List of figures

Suda, et al

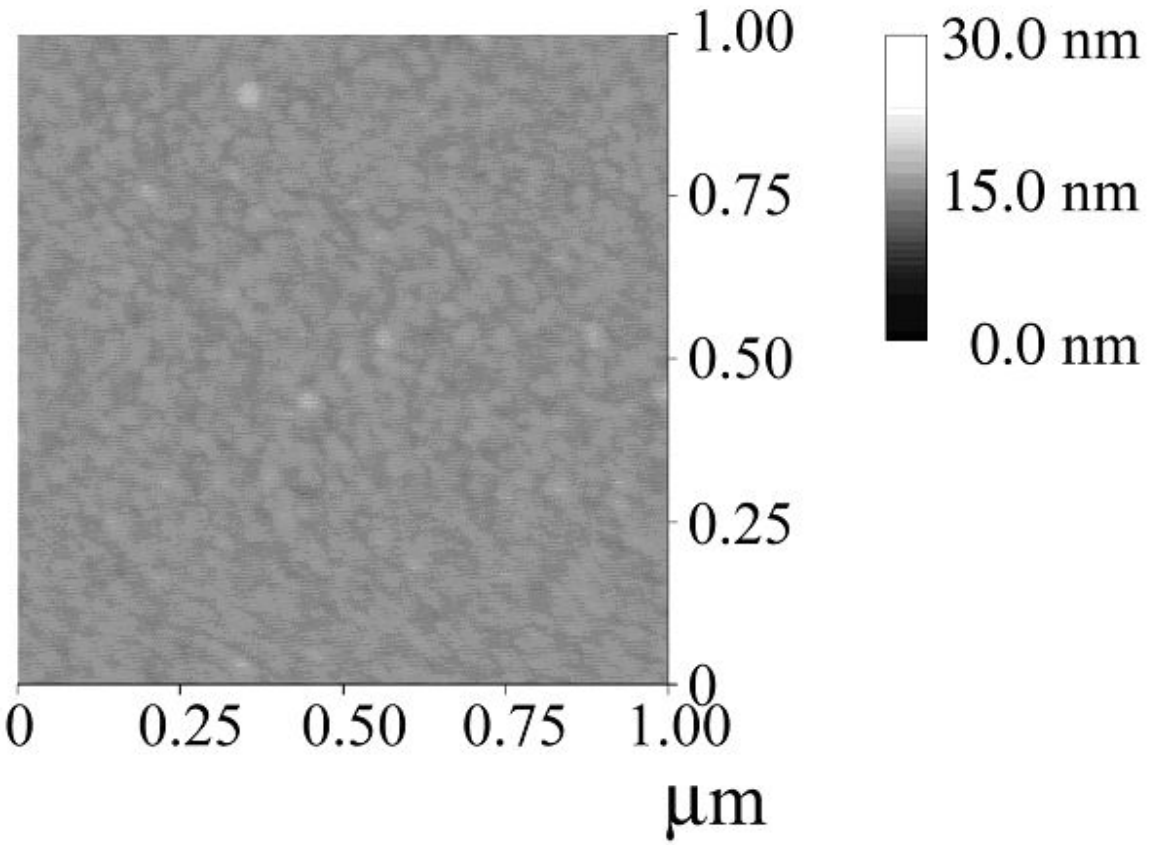

Fig. 1.

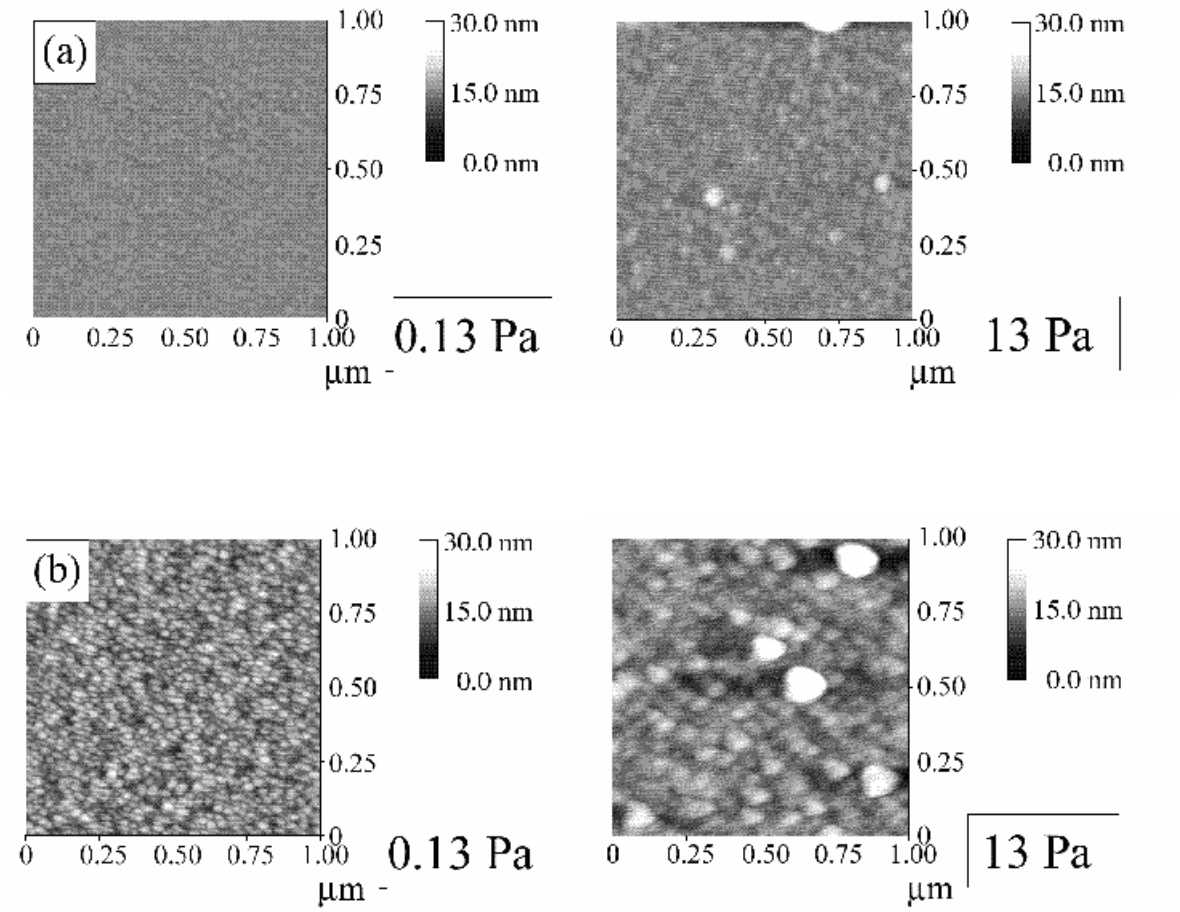

Fig. 2.

Suda, et al

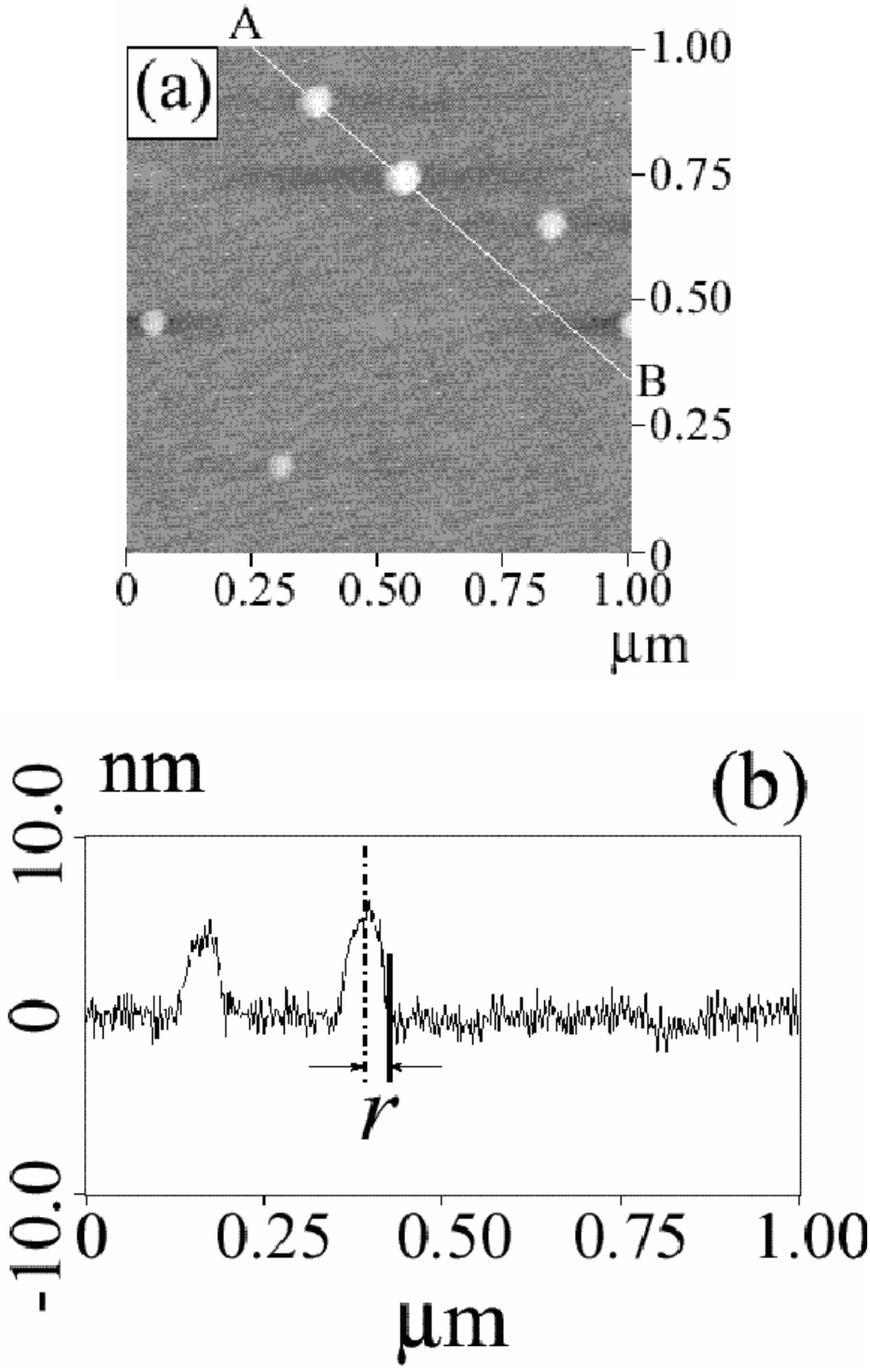

Fig. 3.

Suda, et al

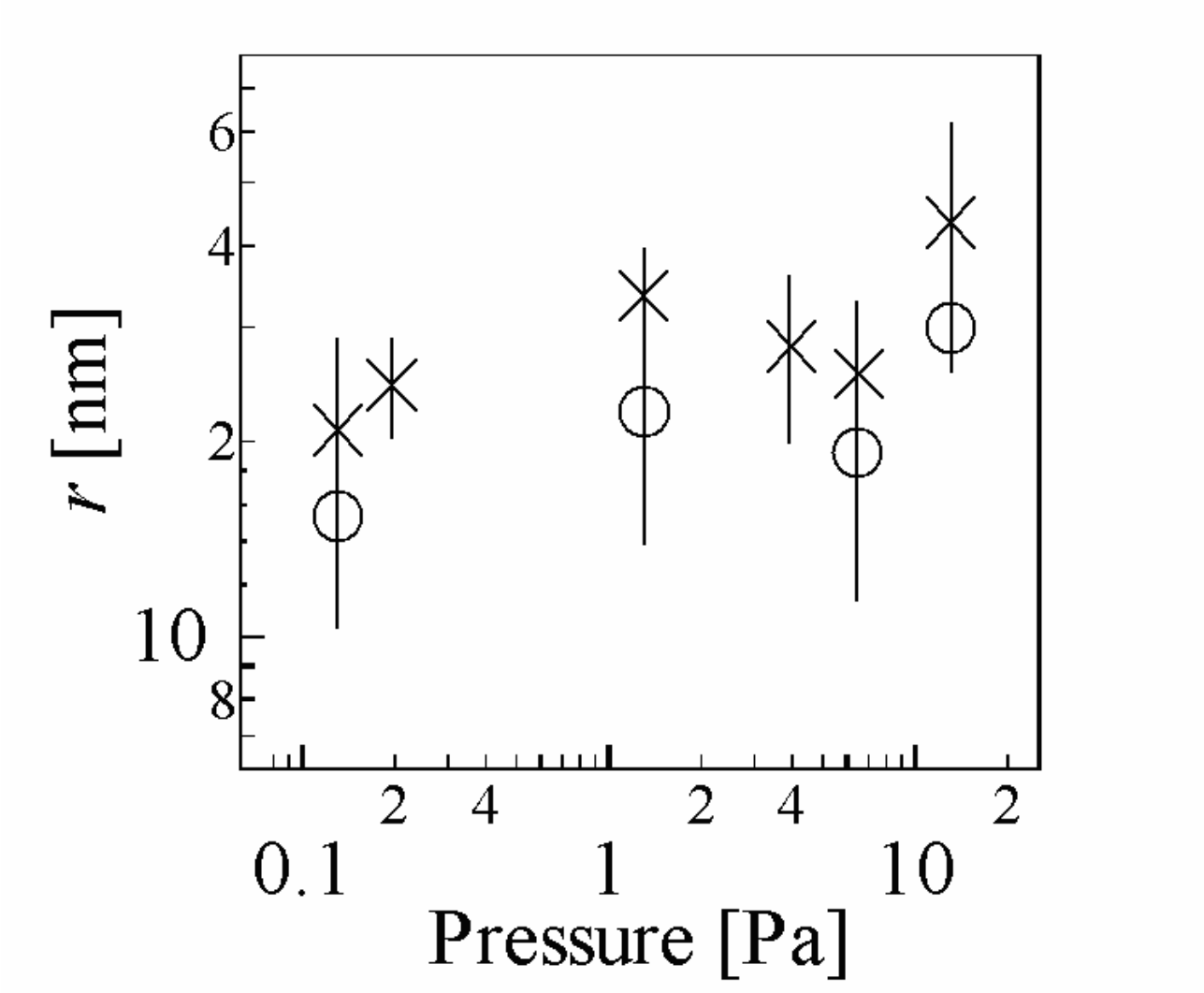

Fig. 4.

Suda, et al

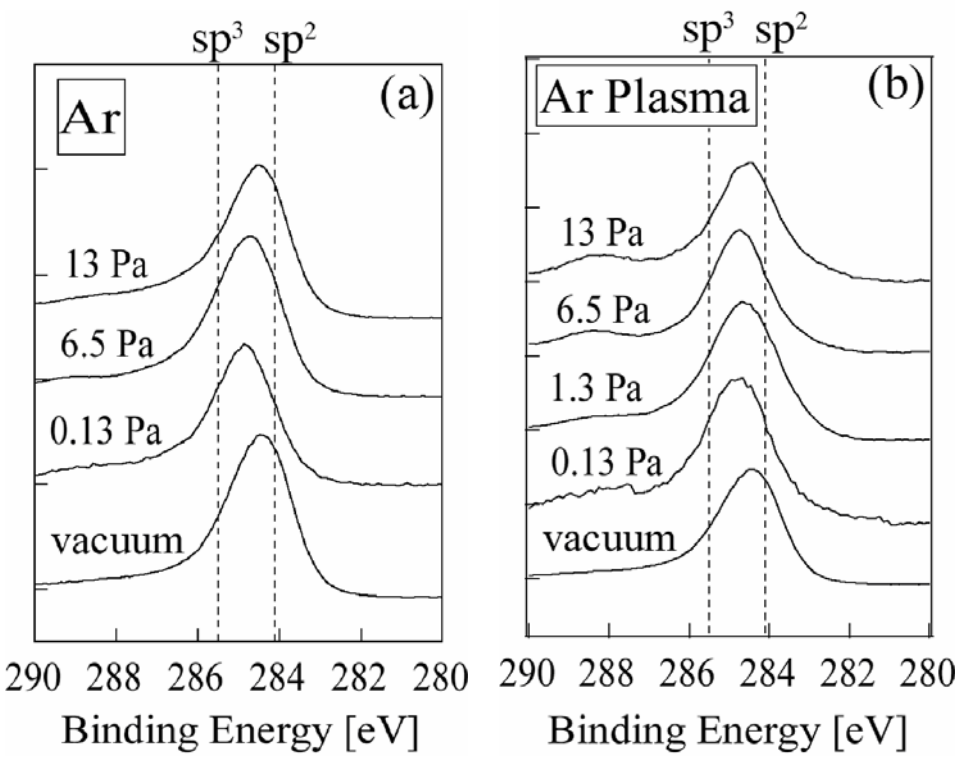

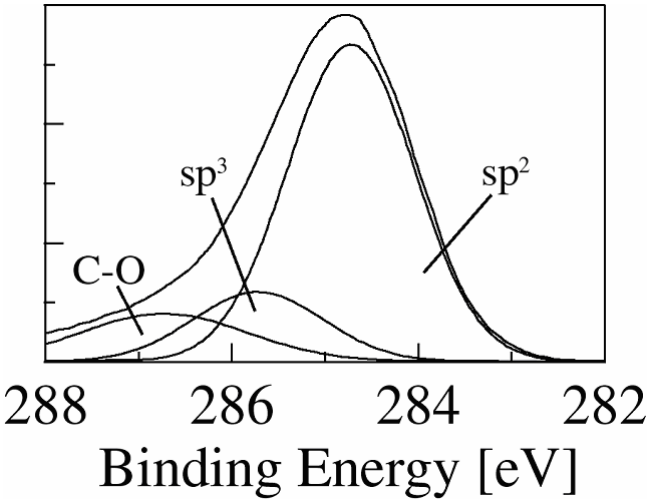

(c)

Fig. 5.

Suda, et al

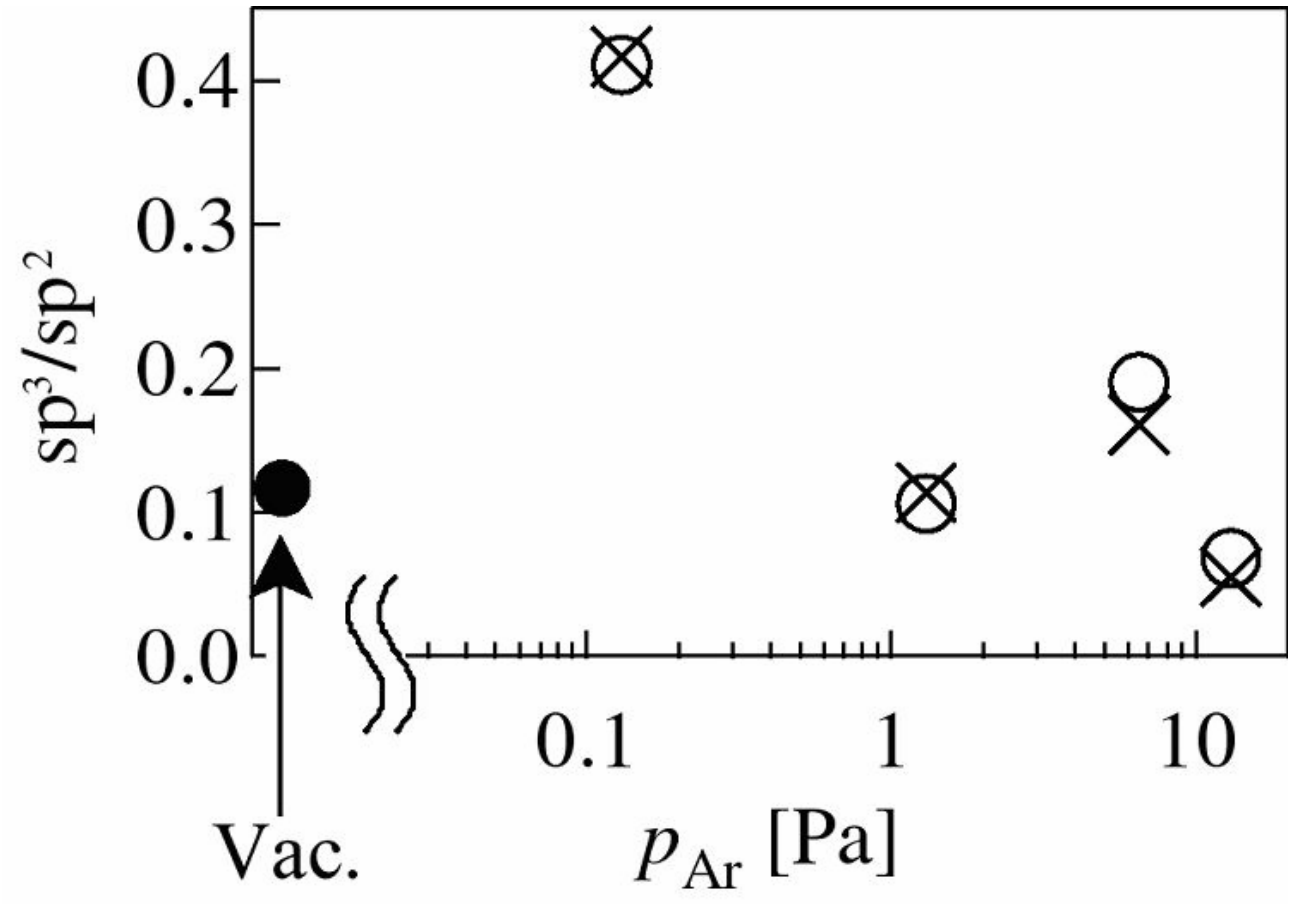

Fig. 6.

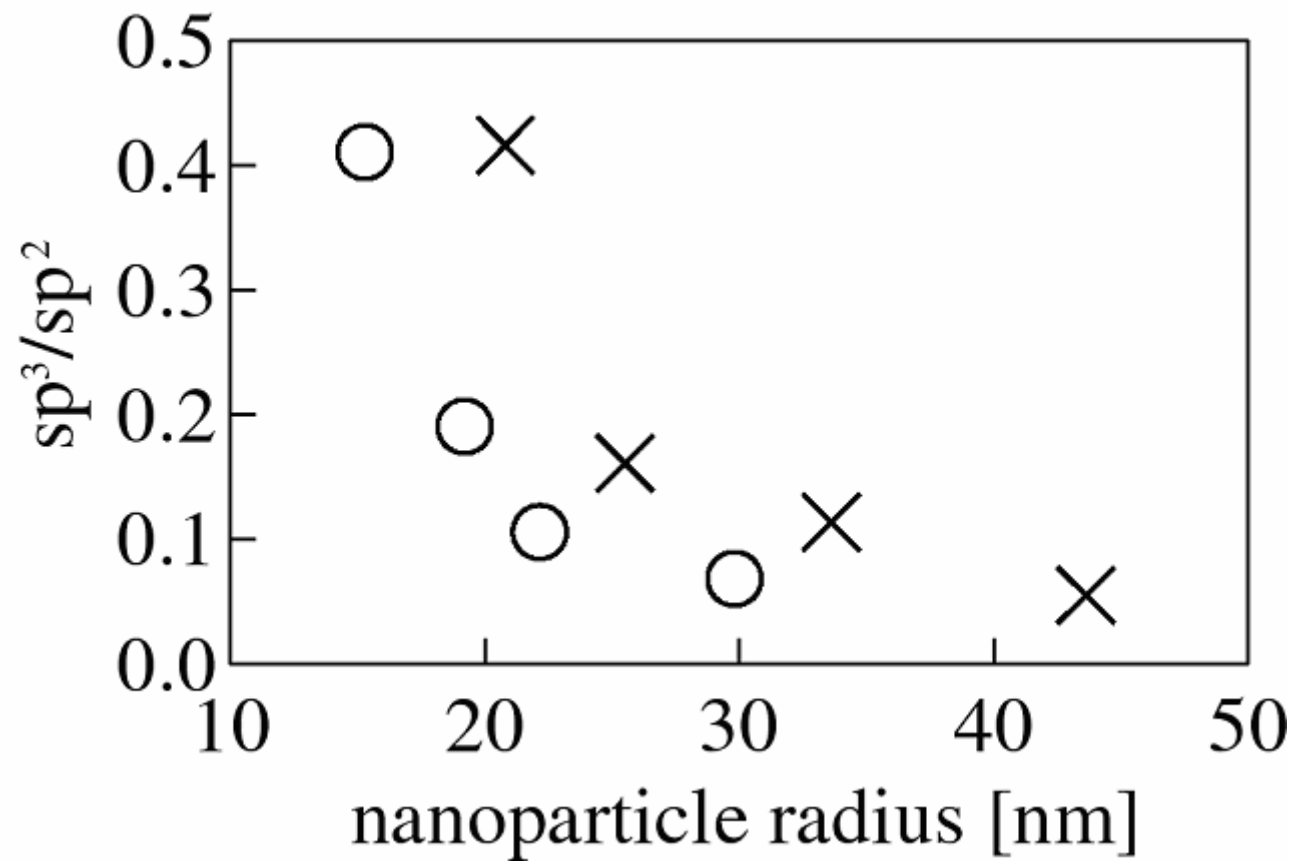

Fig. 7.

Suda, et al